Anticlockwise Rotation, Eccentricity and Tilt Angle of the Wind Hodograph. Part II: An Observational Study

P. ALPERT

Department of Geophysics and Planetary Sciences, Raymond and Beverly Sackler Faculty of Exact Sciences, Tel-Aviv University, Tel-Aviv, Israel

M. KUSUDA AND N. ABE

Oita National Technical College 870-01, 1666 Oaza-Maki, Oita City, Japan

(Manuscript received 10 May 1983, in final form 19 September 1984)

ABSTRACT

Following the theory of Kusuda and Alpert (Part I), expressions for the eccentricity and tilt angle of the surface-wind hodograph at different latitudes are derived as functions of the amplitude and phase shift of the horizontal thermal force and also of some reasonable frictional parameter. Further, analyses of 47 hodographs in Washington, Oregon and California give the observed tilt angles, eccentricities and senses of rotation. The tilt angle is nearly linearly dependent on latitude. Eccentricities are in general high (0.9–1) and higher friction leads usually to higher eccentricity. However, eccentricity may sometimes be very small (giving a circular hodograph) even with high friction and also very high with low friction; the latter case is primarily due to a phase shift between the horizontal thermal forces.

It is shown that although in general the frequency of ACR (anticlockwise rotation) hodographs decreases northward in the Northern Hemisphere, lower friction may lead to a minimum in ACR frequency at some latitude and this (minimum) latitude moves northward as friction increases. ACR hodographs tend to have slightly higher eccentricities relative to those with clockwise rotation.

The limitations of the Rayleigh friction parameterization are discussed and the horizontal momentum equations are solved with the more accurate K-theory friction parameterization. It is shown that near-surface ACR hodographs turn to become clockwise with increasing altitude.

1. Introduction

Kusuda and Alpert (1983, Part I) introduced a simple analytical theory for anticlockwise rotation (ACR) of the wind hodograph. They showed that the inclusion of a pressure-gradient force which rotates diurnally leads to the possibility of ACR. The theory predicts a much wider group of hodographs, relative to previous theory, which consequently have a wider range of eccentricities and hodograph tilt angles, as well as a different sense of rotation. Those hodographs are obtained as functions of: 1) friction (measured by the Rayleigh constant k); 2) relative amplitudes A/B of the thermal forces in the x- and y-directions; 3) the phase shift θ between the thermal forces; and 4) the latitude ϕ.

It might seem that with the aforementioned four variables, every shape of hodograph is possible. However, it will be shown that for realistic values of friction and forcing amplitudes only a small subgroup of hodographs emerges. The specific characteristics of this subgroup are discussed and compared to the parallel features which are found in observed hodographs. Comparisons with the complex shapes of observed hodographs are possible only through detailed harmonic analyses. These analyses were done for two different geographical regions: the Pacific Northwest, including the Columbia Basin of eastern Washington and Oregon, and western Washington and southern Vancouver Island (data from Staley, 1957, 1959); and central California (data from Fosberg and Schroeder, 1967). There are many other hodograph studies for different regions, including those of Frizzola and Fisher (1963) in the New York City area, Weber (1978) in southwest lower Michigan, Barbato (1978) in Boston, Gill (1968) in northeast Scotland, and Zambakas (1973) in Athens. All of these studies show ACR, but as we were primarily interested in studying the variable shapes of hodographs and their average characteristics within some restricted region, only the studies in the western United States were found to be suitable. Staley (1957, 1959) and Fosberg and Schroeder (1967) show relatively large numbers of hodographs, enabling us to deduce their average characteristics in that region.

In Section 2 the analytical expressions and curves for hodograph eccentricity and tilt angle are evaluated and discussed. The analyzed data are presented and compared with theory in Section 3. In Section 4 the predicted frequency of ACR for different latitudes is

introduced, and the few observational results are related to the theoretical curves. Then, in Section 5 we discuss the limitations of the Rayleigh friction theory, solve the set of horizontal momentum equations with the K-theory parameterization, and discuss an ACR example within this theory.

2. Hodograph shape—eccentricity and tilt

Kusuda and Alpert (1983) solved the following set of linear horizontal momentum equations in the x and y directions:

$$\frac{\partial u}{\partial t} - fv + ku = F_x - F_1(t), \tag{1}$$

$$\frac{\partial v}{\partial t} + fu + kv = F_y - F_2(t), \tag{2}$$

where F_x and F_y are forces due to the large-scale pressure gradient, k is constant for the Rayleigh-friction force, and

$$F_1(t) = \frac{A}{\pi} + \frac{A}{2}\cos\omega t, \tag{3}$$

$$F_2(t) = \frac{B}{\pi} + \frac{B}{2}\cos(\omega t - \theta), \tag{4}$$

where A and B are forcing amplitudes in the x- and y-directions, ω is the angular speed of the earth's rotation, and θ is the phase shift between the two forces. Solution of (1) and (2) leads to velocity components u and v which consist of constant components plus components oscillating with time. Of concern here are the transformed values $\tilde{u}$ and $\tilde{v}$ which exclude the constant components.

The hodograph generated by u and v is always an ellipse which may be described by (see Appendix A)

$$\tilde{u} = u_0 \sin(\omega t + \lambda_u), \tag{5}$$

$$\tilde{v} = v_0 \sin(\omega t + \lambda_v), \tag{6}$$

where u_0, v_0 and λ_u, λ_v are velocity and phase constants, respectively. The angle α_1 between the axis of the ellipse and the u-direction is given by

$$\tan 2\alpha_1 = \frac{2u_0v_0}{u_0^2 - v_0^2}\cos(\lambda_u - \lambda_v). \tag{7}$$

After some algebra it may be shown that

$$\tan 2\alpha_1 = 2\,\frac{(A^2 - B^2)fk + AB(f^2 - \omega^2 - k^2)\cos\theta}{(A^2 - B^2)(f^2 - \omega^2 - k^2) - 4ABfk\cos\theta}. \tag{8}$$

For consistency we shall refer to the tilt angle of the hodograph, α, as that angle which the *major* axis makes with the u-direction (i.e., relative to the east) and with the *smallest absolute value*. Following this definition and the requirement that $0 < \alpha_1 < 90°$, it can be shown (see Appendix B) that

$$\alpha = \alpha_1, \qquad \text{for} \quad [\cos(\lambda_u - \lambda_v)] > 0,$$

$$\alpha = \left(\alpha_1 - \frac{\pi}{2}\right), \qquad \text{for} \quad [\cos(\lambda_u - \lambda_v)] < 0,$$

$$\alpha = 0, \qquad \text{for} \quad [\cos(\lambda_u - \lambda_v)] = 0.$$

In other words, in the second case the positive angle α_1 is relative to the minor axis of the ellipse and the transformed negative value α is relative to the major axis.

Also, the eccentricity of the ellipse e, defined as

$$e = (a^2 - b^2)^{0.5}/a,$$

where a and b are the semimajor and semiminor axes of the ellipse, may be shown to obey the relation

$$e = \left\{\frac{2|[(A^2 - B^2)(f^2 - \omega^2 - k^2) - 4ABfk\cos\theta]\sec 2\alpha_1|}{(A^2 + B^2)(f^2 + \omega^2 + k^2) - 4ABf\omega\sin\theta + |[(A^2 - B^2)(f^2 - \omega^2 - k^2) - 4ABfk\cos\theta]\sec 2\alpha_1|}\right\}^{1/2}. \tag{9}$$

The derivation of the expressions for e and α is described in Appendix C. The values of e and the tilt angle α of the major axis of the ellipse (as well as the sense of rotation discussed in the last section), which are predicted by the theory, may be tested readily against observed data. In order to do such a test, the characteristics of α and e will be illustrated by some figures.

Figure 1 shows α and e as functions of northern latitude for $k/\omega = 0,\ 0.1,\ 0.5,\ 1,\ 2,\ \infty$, for the limiting case where the thermal forcing in the y-direction vanishes, i.e., $B = 0$. In fact, this is exactly the case studied by Haurwitz (1947). Equation (8) thus simplifies to

$$\tan 2\alpha_1 = 2fk/(f^2 - \omega^2 - k^2), \tag{10}$$

and for the special case, $k = \omega$, it simplifies further to

$$\tan 2\alpha_1 = \tan(-2\phi)/\cos\phi. \tag{11}$$

Since the sign of $\{\cos(\lambda_u - \lambda_v)\}$ is negative (see Appendix B), $\alpha = (\alpha_1 - \pi/2)$ and the tilt angle α must be negative (positive in the Southern Hemisphere). Another interesting feature is the quasi-linear dependence of the tilt angle α upon the latitude over a wide range of friction values. For low latitudes (11) could be approximated by

$$\alpha \simeq -\phi, \tag{12}$$

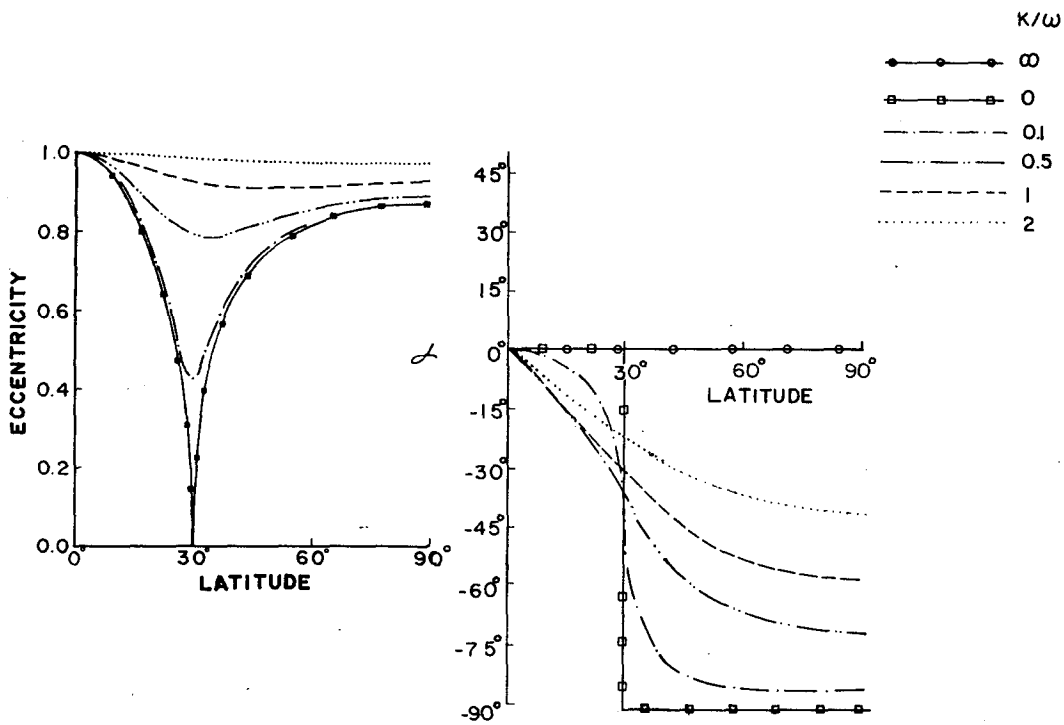

FIG. 1. Eccentricities e and tilt angles α of hodograph major axes as functions of northern latitude for $k/\omega = 0$, 0.1, 0.5, 1, 2, ∞, for the case where the second thermal forcing is zero ($B = 0$, $A = 0.04$ cm s^{-2}).

i.e., the tilt angle of the ellipse α is equal to the negative value of the latitude angle. This explains rather clearly why Haurwitz (1947) predicted a value of about $-45°$ for the tilt angle of a hodograph at $\sim 43°$ latitude. His values of k/ω were ~ 0.78 or ~ 1.37, which do not change significantly the latitude dependence illustrated in Fig. 1.

Figure 1 also shows that for reasonable[1] values of k, hodographs are expected to have relatively high eccentricities. As discussed by Haurwitz (1947), the eccentricity in that simple case became higher as the friction increased.

Figures 2a–c illustrate the same features for the more general case with $A = B \neq 0$, i.e., two thermal forcings are present in the horizontal, having the same amplitude but some phase shift θ between them. The three figures correspond to different frictions, $k/\omega = 0$, 1 and 2. Here (8) simplifies to

$$\tan 2\alpha_1 = -(f^2 - \omega^2 - k^2)/2fk. \qquad (13)$$

The tilt angle α becomes independent of the phase shift θ. As before (for $B = 0$), there is an approximate linear dependence between α and the latitude ϕ. For $k = \omega$ we have

$$\tan 2\alpha_1 = \cos\phi/\tan(2\phi), \qquad (14)$$

which in turn yields

$$\alpha = \alpha_1 \approx 45 - \phi. \qquad (15)$$

This approximation is found to be very good for latitudes up to about 50°N (see Table 1).

Contrary to the former case ($B = 0$), here the tilt angle is positive for lower latitudes and even more so for higher friction (Figs. 2b and c). Again, the eccentricities are relatively high but the increase of friction does not necessarily increase the eccentricity. In fact, the opposite happens for large phase shifts, e.g., for $\theta = 80°$. Notice also the circular hodographs ($e = 0$) for phase shifts of 90°, which are independent of friction and latitude.

It is interesting to note the discontinuity at 30° latitude in the limiting case where friction becomes zero. At that point, i.e. $f = \omega$, which is predicted by the change of sign in $\cos(\lambda_u - \lambda_v)$, the ellipse becomes a circle, i.e., $e = 0$. When $k = \omega$, the change in sign of α is continuous (Fig. 2b) and is predicted to happen at 45° latitude where $f^2 = 2\omega^2$ (see Appendix B).

The even more general case where $A \neq B \neq 0$ is illustrated in Figs. 3a–c for $A/B = 2$ with the friction parameters $k/\omega = 0$, 1 and 2. Now the tilt angle of the hodograph depends upon the shift angle θ and becomes smaller (more negative) for larger θ. There is still a nearly quite linear dependence of α upon

[1] These are based on the range of k-values ($0.2–0.8 \times 10^{-4}$ s^{-1}) given by Haurwitz (1947) which correspond to $k/\omega \approx (0.3–1.1)$, from which the smaller values of k are found near the coast or over the ocean. Thus, k/ω values over continents should be in the range of $\sim 0.6–1.1$.

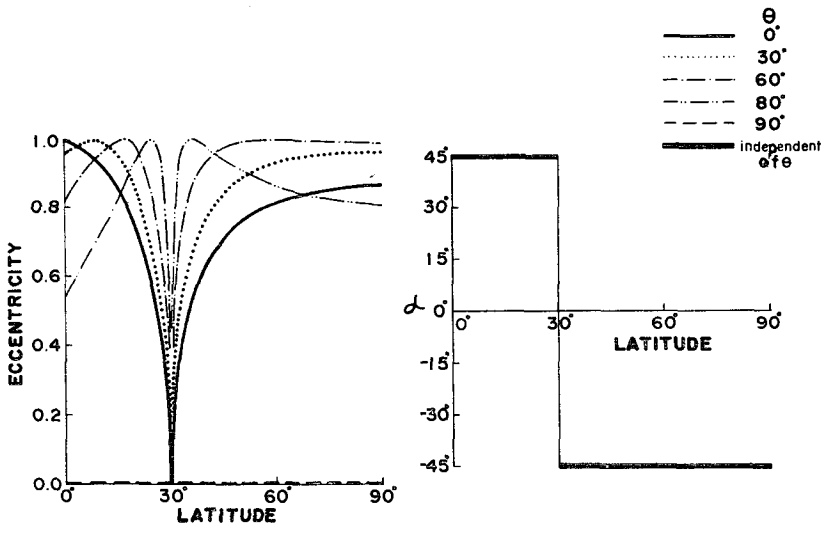

FIG. 2a. As in Fig. 1 but for $k/\omega = 0$ (no friction) and different values of the phase shift $\theta = 0$, 30, 60, 80 and 90. Here, both horizontal forcings have the same amplitude ($A = B$). The heavy line represents the curve when it is independent of θ.

latitude at lower latitudes except for the discontinuity at 30°N for $k = 0$. The eccentricities are even higher here and are usually greater than 0.9 for the viscous solutions. Notice that unlike the former case ($A = B$) in which a phase shift of 90° led to circular hodographs, here even that phase-shift leads to high eccentricities.

The effect of any further decrease in the thermal-forcing amplitude in the y-direction is not illustrated because the graphs are very similar to the preceding figures. It should be mentioned, however, that the phase-shift dependence of both α and e decreases considerably in this case, and in fact the figures start to resemble the limiting case for $B = 0$, i.e., Fig. 1.

To illustrate some of the aforementioned features, Fig. 4a shows four hodographs predicted for latitude 45°N, a phase shift of 40° and equal horizontal forcing amplitudes, i.e., $A = B$, for four different friction parameters $k/\omega = 0$, 0.5, 1 and 2. Of course, the increase in friction diminishes the average wind speed but does not necessarily increase the eccentricity. For example, the eccentricity for the ACR case with $k/\omega = 2$ is lower than the eccentricity with $k/\omega = 1$. Also, the figure shows that higher values of k lead to larger α. Figure 4b is similar but for $A/B = 2$, and illustrates how it becomes more difficult to get ACR as the second forcing becomes smaller.

The strong influence of the phase shift upon the sense of rotation is shown in Fig. 4c, where $k = \omega$, $\phi = 45°$ and $A = B$. Notice how the CR hodograph for a zero phase-shift angle, i.e., $\theta = 0$ (dash-dot line), becomes a line hodograph coinciding with the $\tilde{u}$ axis for $\theta = 45°$ (eccentricity = 1), and then becomes an ACR hodograph (full line) at $\theta = 90°$. As anticipated

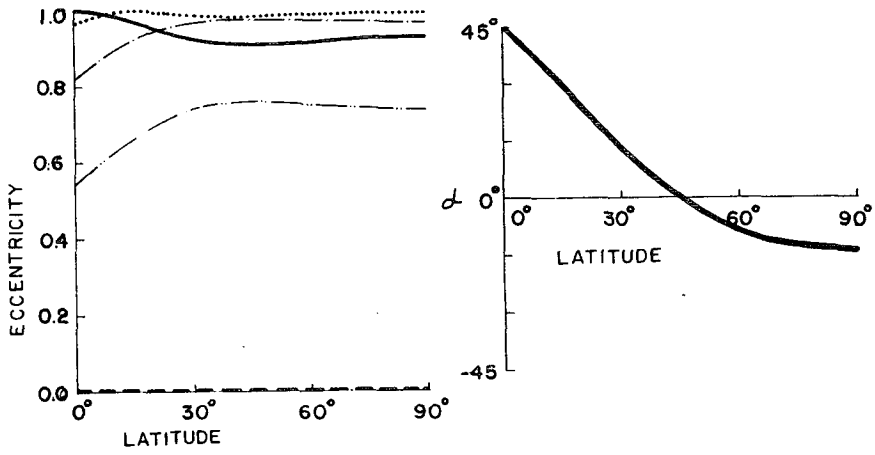

FIG. 2b. As in Fig. 2a but with $k/\omega = 1$.

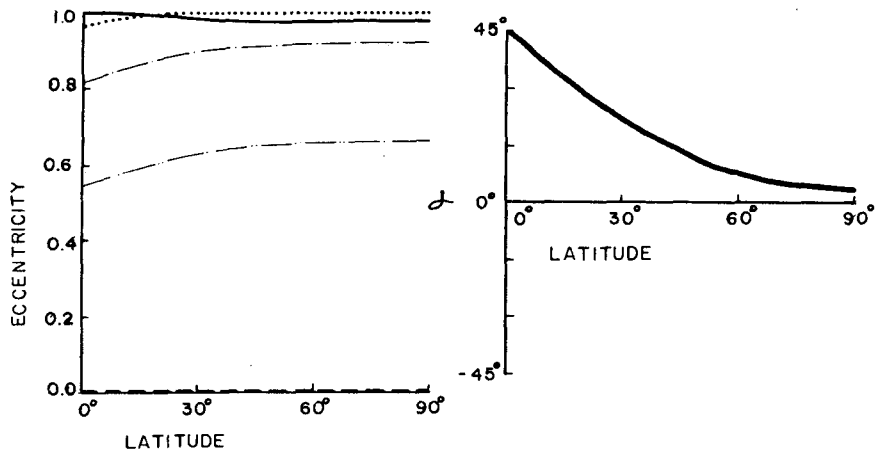

FIG. 2c. As in Fig. 2a but with $k/\omega = 2$.

from Fig. 2b, the three hodographs are all oriented such that the major axes of the ellipses coincide with the $\tilde{u}$ coordinate. For reference, the CR hodograph for $B = 0$ at the same latitude ($\phi = 45°$N) (double dot-dash line) and the ACR hodograph at the equator for $\theta = 90°$ (dashed line) also are shown. The hodograph corresponding to the Haurwitz (1947) theory with no second forcing (double dot-dash line) has a tilt $\alpha = -45°$ at $\phi = 45°$N as predicted by (12). However, when a second equal forcing also is taken into account, the predicted tilt angle at the same latitude is very different, i.e., $\alpha = 0°$ as predicted by (15). Also, the different phase shifts with the second forcing may lead to variable ellipse eccentricity as illustrated in Fig. 4c and predicted by the eccentricity formula (see Fig. 2b).

3. Shapes of observed hodographs in light of the theory

Average summer hodographs of resultant surface winds for 26 stations in and near Washington state (data from Staley, 1957, 1959) and 21 stations in central California (data from Fosberg and Schroeder, 1966) were analyzed. In a harmonic analysis for each hodograph, the first-order ellipse was chosen. The spatial fields of the observed eccentricities and tilt angles are shown in Figs. 5 and 6, respectively.

TABLE 1. Predicted hodograph tilt angles α as functions of latitude ϕ for the case where the amplitudes of the horizontal forcings are equal ($A = B$) and the friction parameter k is equal to ω. Equation (14) gives the exact angle predicted by theory, while Eq. (15) is the approximate formula for low and middle latitudes.

ϕ	α [Eq. (14)]	$\alpha = 45 - \phi$ [Eq. (15)]
0	45	45
10	34.8	35
20	24.1	25
30	13.3	15
40	3.8	5
45	0	0
50	−3.2	−5
60	−8	−15
70	−11.1	−25
80	−12.8	−35
90	−13.3	−45

The first striking fact shown by Fig. 5 is the very high observed eccentricity, with averages of 0.898 and 0.946 for the stations in Washington and California, respectively. Note, however, that the *predicted* eccentricities for the more realistic cases, i.e., $k/\omega = 1$, are approximately the same (see Figs. 1, 2b and 3b). It is difficult to relate exactly the small decrease in observed average eccentricity with latitude based only on these two regions, i.e., the change from 0.946 to 0.898 moving from ~38° to ~47°. However, a similar decrease might be found for $k = \omega$ at small phase-shift angles (see Fig. 1 for $B = 0$ and Fig. 2b where $A = B$ for $\theta = 0$). It should be stated, however, that the slight change in average eccentricity between the two regions might be of no significance for the latitude dependence since changes in local friction and the relative intensities of thermal forcings may play an important role for such a relatively small number of observational points. Obviously, as the data base becomes larger and includes more latitudes, a more quantitative comparison might be possible. That comparison will show to what extent the linear theory could be applied to studies of hodograph shape.

The data for the tilt angles of the analyzed hodographs (Fig. 6) are somewhat more complex, and so conclusions cannot immediately be drawn. Figure 7 shows histograms for the frequency of tilt angles α with intervals of 30°. These show that the preferred interval in Washington (~47°N) is $\alpha = 0$ to −30°, while in central California (~38°N) it is 0 to 30°. These results again seem to be in agreement with the predicted tilt angles for $k = \omega$ and $A = B$ (see Fig. 2b). An increase in the data base should, of course,

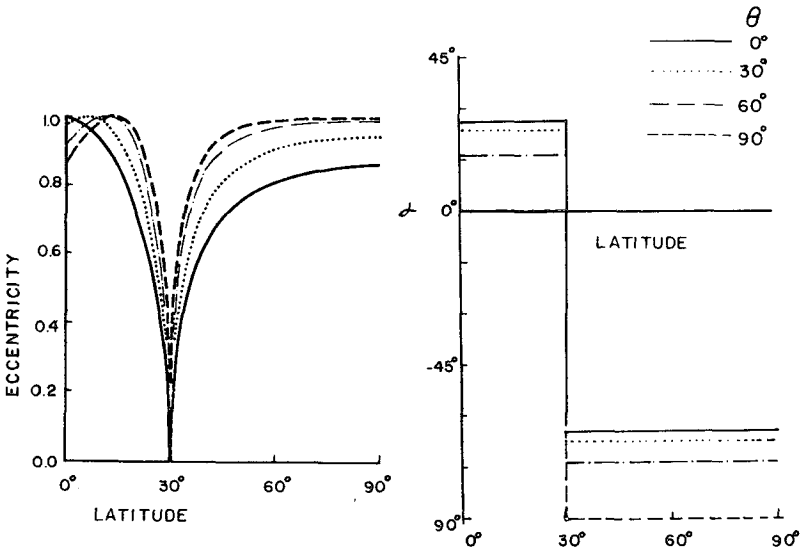

FIG. 3a. As in Fig. 2a but $A/B = 2$.

allow a better comparison. These results imply that on the average, in analyses of observed hodograph shapes, equal amplitudes of thermal forces in both horizontal directions (i.e., $A = B$) might be suitable in the analytical derivation. We suggest that this is because the average thermal forcing in areas of appreciable variability in meso- and microscale features will usually not prefer one direction above the other.

Recently, we analyzed 12 additional hodographs in central California based upon data for July 1958 from Frenzel (1962). The results (not shown) indicate a high average eccentricity of 0.94, which is especially pronounced for the ACR hodographs (see the next section and Table 2). The tilt angles of the hodographs are mostly negative, weakening the preference for positive α values in the California histogram. The new totals for the 30° intervals of the California histogram for 33 hodographs are (from left to right) 1, 8, 9, 11, 4 and 0, respectively. Of course, we still have the maximum of 11 hodographs in the 0 to 30° interval but more hodographs show negative tilt angles. This was correctly anticipated by D. O. Staley (personal communication, 1983), based upon the orientation of the central valley of California.

Staley (1957) summarized some of the features of observed hodographs in light of the Haurwitz (1947) theory. Two of his main observations are (quoting from his paper):

1) "Counter-clockwise rotation at certain stations."

2) "Nearly circular hodographs in the northern and central Puget Sound. According to Haurwitz' theory, the eccentricity of the elliptical hodographs depends directly on friction, but it is improbable that this area offers no frictional resistance. Also, topo-

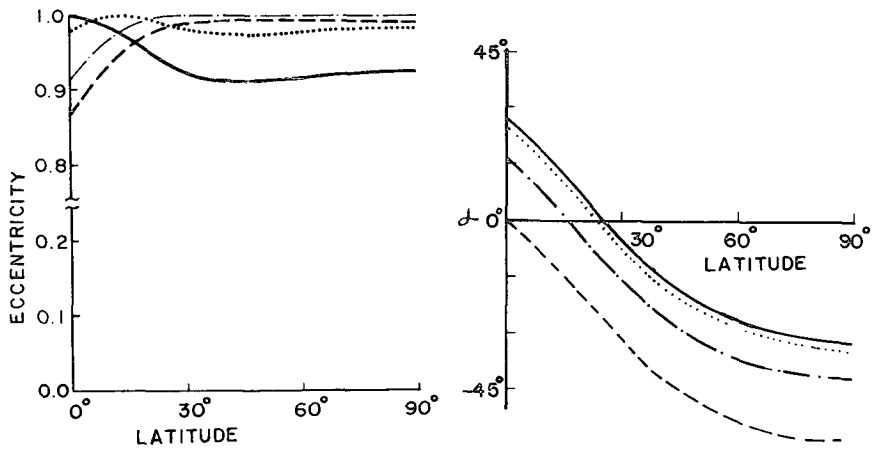

FIG. 3b. As in Fig. 2b but with $A/B = 2$.

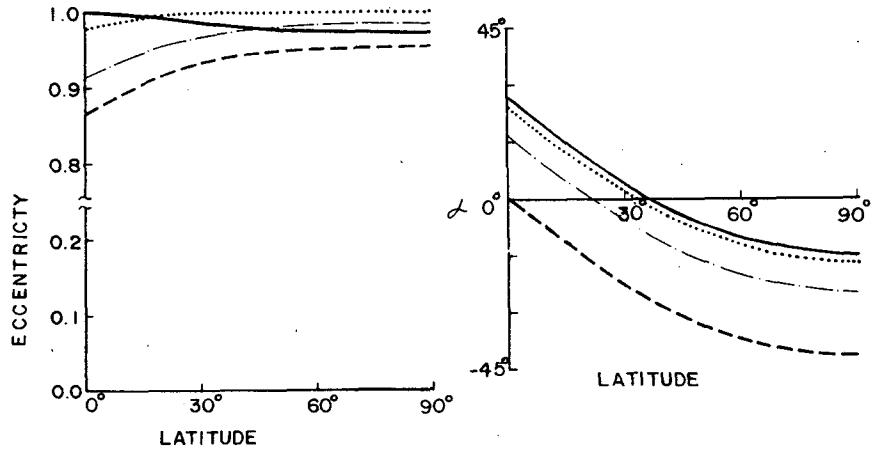

FIG. 3c. As in Fig. 2c but with $A/B = 2$.

graphical constraint, if any, would be expected to elongate the hodograph."

The present theory suggests a simple explanation of these features through the presence of a rotating horizontal pressure-gradient force which was in fact suggested by Staley (1957). The counterclockwise rotation is predicted by this theory. Also, the nearly circular hodographs that were observed over Puget Sound with the low eccentricities of 0.54, 0.68 and 0.60 (see Fig. 6) are possible with realistic values of friction if a relatively large phase shift exists (see Figs. 2b and c). In fact, as pointed out before, the increase in friction sometimes might even *decrease* the eccentricity of the ellipse. This is illustrated by a comparison of the eccentricity curves for the phase shift $\theta = 80°$ in Figs. 2b and c.

4. The frequency of anticlockwise rotation at different latitudes

An interesting result of this study is that in the Northern (Southern) Hemisphere, northward (southward) movement does not necessarily increase the chance of CR (ACR) for reasonable values of friction. An increase might have been expected since the Coriolis effect increases poleward. However, the linear theory suggests the existence of a minimum probability for ACR (CR in the Southern Hemisphere) for some latitude depending upon the local friction. As the friction increases, this latitude of minimum ACR (CR) moves northward (southward). Figure 8 shows the predicted frequencies of ACR (CR) hodographs as functions of northern (southern) latitude for four different cases. The numbers of ACR and CR occurrences are n_1 and n_2, respectively. Curves 1 and 2

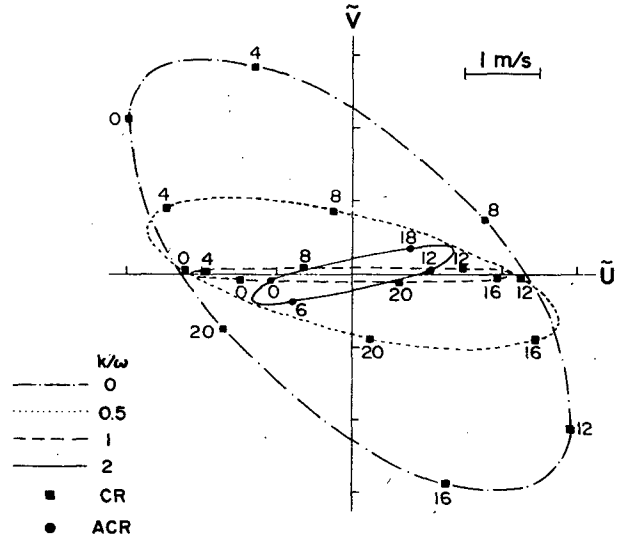

FIG. 4a. Predicted hodographs for latitude $\phi = 45°$N, a phase shift of 40° and equal horizontal forcing amplitudes, i.e., $A = B$, for four different friction parameters $k/\omega = 0$, 0.5, 1 and 2.

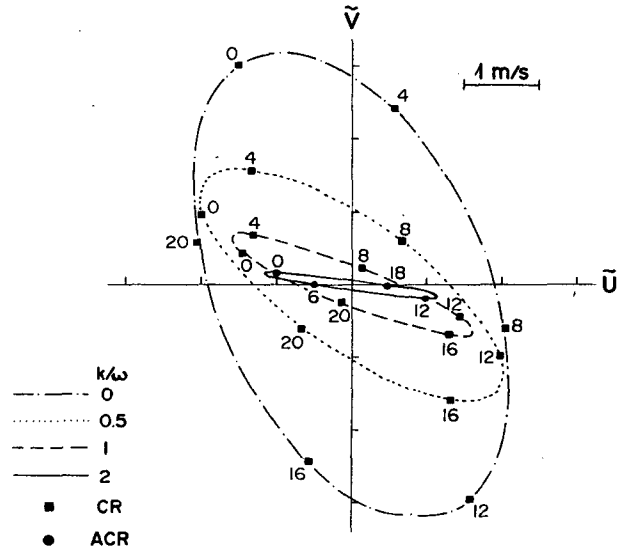

FIG. 4b. As in Fig. 4a but for $A/B = 2$.

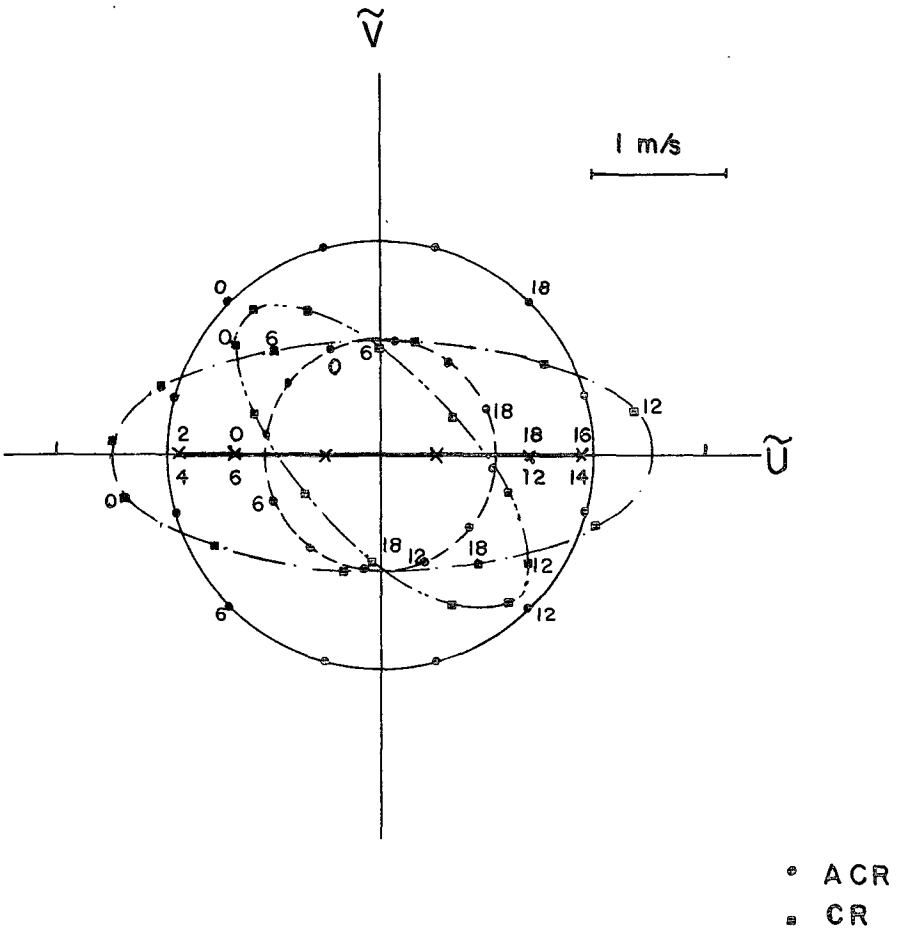

FIG. 4c. Some hodographs which illustrate dependence upon phase shift θ. Three of the hodographs are for 45°N, $k/\omega = 1$ and $A = B$ as follows: Dot-dashed line: $\theta = 0$. Heavy solid line: $\theta = 45°$. Light solid line: $\theta = 90°$. The two additional hodographs are for 45°N latitude, $k/\omega = 1$ and $A/B = 2$ (dot-dot-dashed line), and for the equator, $k/\omega = 1$ and $A = B$ (dashed line). ACR and CR hodographs are indicated by solid dots and squares, respectively.

represent two cases with reasonable values of friction ($k = \omega$) for which A/B changes from 1 to ~2.4. As this proportion increases ($B \rightarrow 0$, approaching the Haurwitz case), ACR disappears first in middle latitudes, then in the northern latitudes (not shown in Fig. 8) and finally in lower latitudes, thus leaving the Northern Hemisphere free of ACR for $B = 0$. Curve 3, for $A = B$ but higher friction ($k \sim 1.73\omega$), illustrates (compare to curve 1) how the increase in friction leads to a gradual decrease in the ACR frequency with latitude. Curve 4, where $A = 3.7B$ and $k = 1.73\omega$, shows a decrease similar to curve 3 but the absolute values of ACR frequency are considerably smaller, particularly in northern latitudes; this is due to the relative reduction of the second forcing. These curves are based upon the ad hoc assumption of a constant probability distribution for different phase shifts in the full region ($-180° < \theta < 180°$). It might be argued that the more realistic probability distribution will indicate a maximum at zero phase shift and a decreasing probability with increasing phase shifts, i.e., increasing $|\theta|$. Such an argument could be verified only through a comprehensive analysis of the different thermal forcings observed in as many different locations as possible. If that argument is found to be correct, the predicted frequency for ACR will be reduced by an appreciable factor because small phase shifts do not support ACR. In any case, for a given latitude the curves in Fig. 8 at least suggest some upper bound to the number of ACR occurrences, n_1, relative to the total number of observed hodographs, $(n_1 + n_2)$.

If we adopt the aforementioned suggestion (see Section 3) that $A = B$, and choose a reasonable friction parameter, then curves 1 and 3 would be the potential curves for comparison with observations.

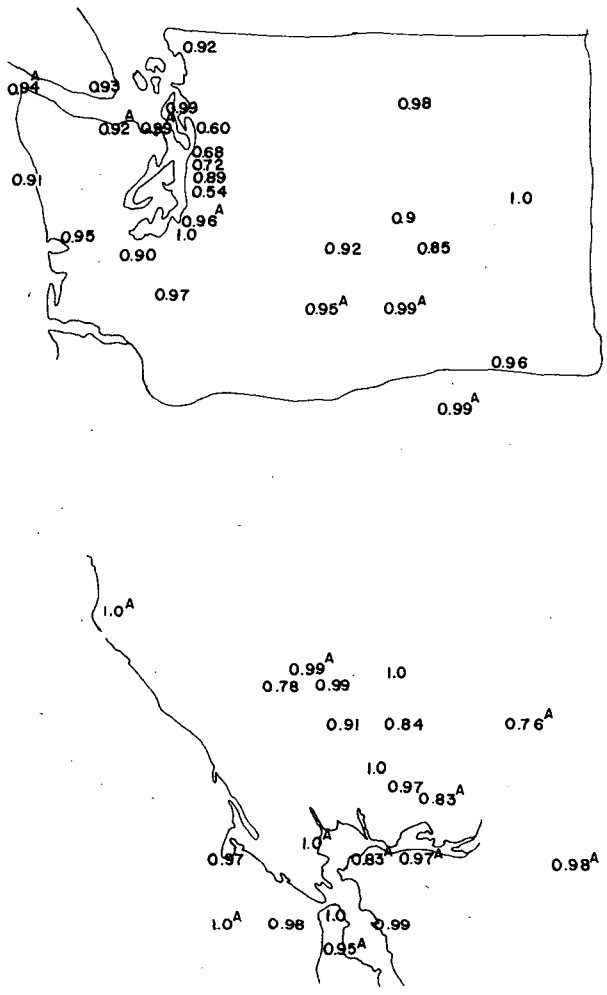

FIG. 5. Fields of observed eccentricities for the Pacific Northwest (top) and California (bottom). Results are based on harmonic analyses of the observed hodographs of Staley (1957, 1959) and Fosberg and Schroeder (1966). Hodographs with ACR are denoted by "A." Other hodographs show clockwise rotation.

In a recent study in Japan (Mori, 1982) entailing harmonic analysis of about 100 stations, one third of the stations showed ACR (j in Fig. 8). (Points C and W in Fig. 8 represent results for the California and Washington hodographs, respectively.) Also, the equal numbers of ACR and CR cases observed near the equator, i.e., at Batavia, Indonesia (Wexler, 1946), supports the value of 0.5 predicted at the equator by all curves. The California point is somewhat distant from our corresponding curves, while the other points seem to be within the predicted region of ACR frequency. Another study by two of the authors (M.K. and N.A.) of 24 hodographs in the restricted area of Oita City, Japan has shown 13 stations with ACR, a relatively high frequency of 0.54. This study was based upon wind data gathered for air pollution purposes and was found unsuitable for use here. Since all of the stations were relatively close to each other they were influenced by similar thermal forcing (the sea, a river and topography) which probably favored ACR. Ratios of ACR to CR frequencies in Washington and California are given in Table 2. Of course, analyses of more data at different latitudes are necessary in order to allow a more extensive comparison with our curves.

Another question which relates to the occurrence of ACR is: Do ACR hodographs tend to be more flattened (have higher eccentricity) than CR hodographs? Table 2 shows average values and standard deviations of observed eccentricities for ACR and CR hodographs in Washington and California. The ACR eccentricity is higher than CR in Washington and central California but lower in western California. The overall picture is that ACR hodographs tend to be slightly more flattened, for our limited set of hodographs.

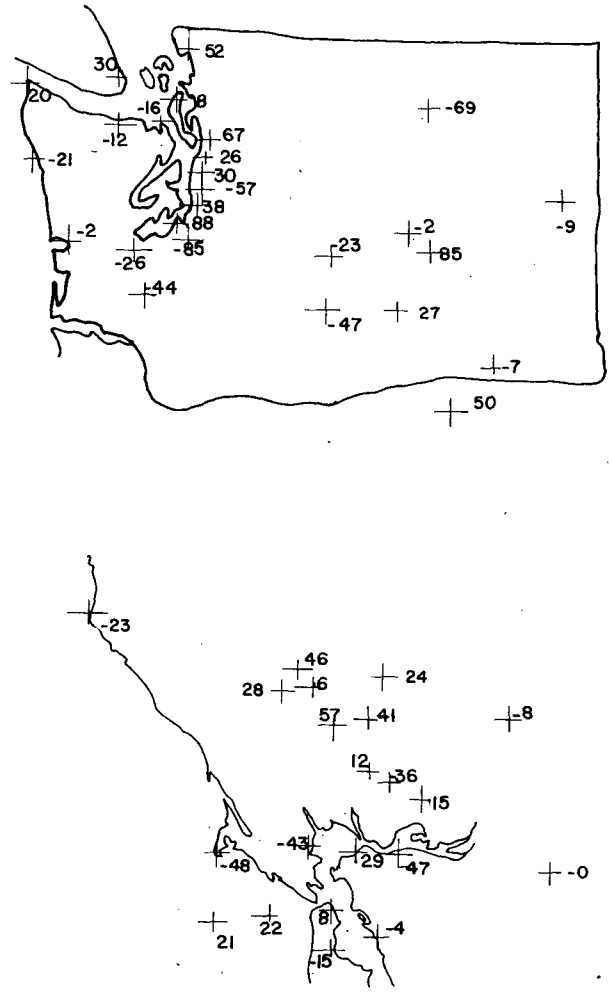

FIG. 6. As in Fig. 5 but showing tilt angles between hodograph major axes and positive directions of the u axes. Crosses show locations of the observations.

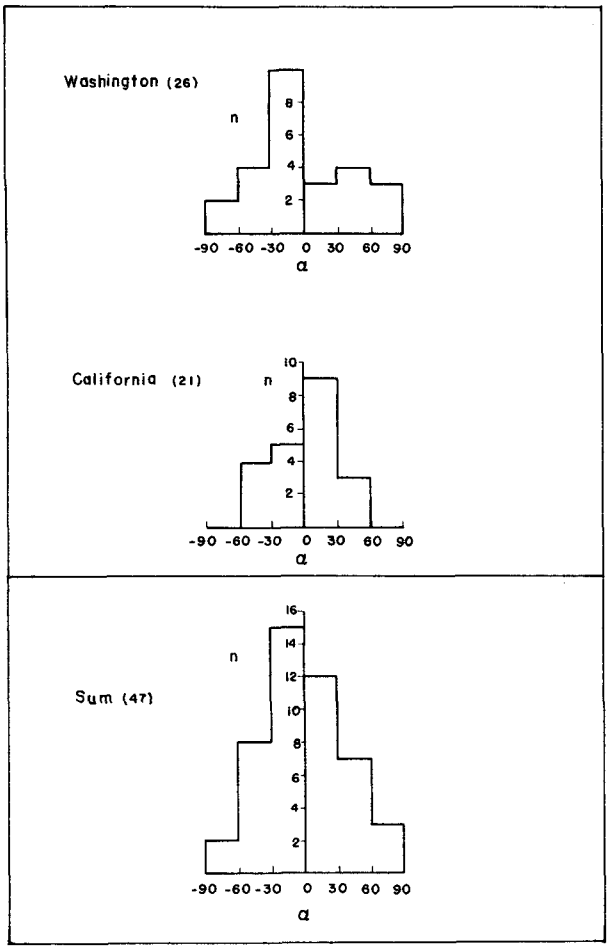

FIG. 7. Histograms showing frequencies of tilt angles α by intervals of 30° for 26 stations in Washington, 21 stations in California, and the sum of both regions. Here n represents the number of observed hodographs at the specific intervals in α.

5. Effects of different parameterizations of the frictional force on the wind rotation

We have dealt here with some of the observed features of the hodograph that we believe the present theory, although highly simplified, may explain. Nevertheless, we question the applicability of this theory, which is based upon parcel dynamics, ignores continuity, thermodynamic energy, the transient terms and nonlinear and linear advection, and assumes simple sinusoidal forcing and a linear Rayleigh friction. We tend to agree with the reviewers, who believe that one of the most serious simplifications in the study of hodograph shape is that of Rayleigh friction. However, it should be mentioned that, using Rayleigh friction, Thorpe and Guymer (1977) succeeded in reproducing some of the basic features of the nocturnal jet. They justified the use of Rayleigh friction by citing previous studies, e.g., Clarke (1970), which showed that for a wide range of situations there exists a linear stress profile in, at least, the surface wind direction. They concluded, therefore, that in general any deviations from linearity are likely to be of little importance for a slab-type model during daytime. At night, however, they concluded that nonlinear effects may be of greater importance. They also compared their results with a model in which the more accurate velocity-square dependence was adopted for the frictional force, and found the results to be an acceptable approximation for the wind evolution.

J. C. Wyngaard (personal communication, 19$$) has recently shown that the frictional contribution to the evolution of the surface wind angle can be written as

$$\left.\frac{d\alpha}{dt}\right|_{\text{frictional}} = \frac{f}{S^2}(V\delta V_a + U\delta U_a), \qquad (16)$$

where s is wind shear, f the Coriolis parameter, and

$$(\delta U, \delta V) = \delta \mathbf{V} = (\mathbf{V} - \mathbf{V}_g) - (\langle \mathbf{V} \rangle - \langle \mathbf{V}_g \rangle).$$

Averaged quantities through the entire height h of the planetary boundary layer (PBL) are denoted by angular brackets, and the subscript g denotes the geostrophic wind.

For a baroclinic, convective PBL, Eq. (16) could be modified to give

$$\frac{d\alpha}{dt} = \frac{fh}{2S^2}\left(V\frac{\partial Vg}{\partial z} + U\frac{\partial Ug}{\partial z}\right) \quad \text{(friction)}$$

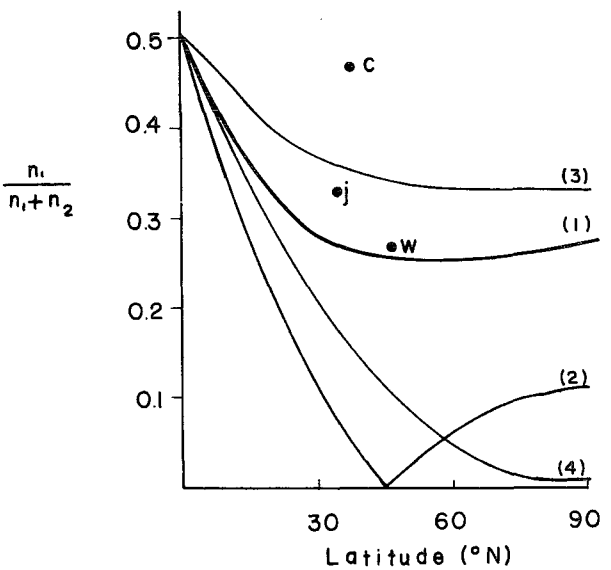

FIG. 8. The predicted frequencies of ACR (CR) hodographs as functions of northern (southern) latitude for four different cases: 1) Friction parameter $k = \omega$ and $A = B$. 2) As in 1) but for $A/B \approx 2.4$. 3) $k = 1.73\omega$ and $A = B$. 4) As in 3 but for $A/B \approx 3.7$. The numbers of ACR and CR occurrences are n_1 and n_2, respectively. Case 1 is shown with a heavier line to indicate that it is the most realistic.

TABLE 2. Average values and standard deviations of observed eccentricities for both ACR and CR hodographs in Washington and California. The numbers of stations in each category are shown in parentheses. The frequency of ACR occurrences in these regions is also shown. Here, n_1 and n_2 are the numbers of ACR and CR hodographs, respectively, observed in each region.

Region	$\frac{n_1}{n_1+n_2}$	Eccentricity		
		ACR	CR	ACR + CR
W Washington	0.27 {0.24	0.95 ± 0.02 (4)	0.85 ± 0.15 (13)	0.87 ± 0.14 (17)
E Washington (Columbia Basin)	0.27 {0.33	0.97 ± 0.02 (3)	0.93 ± 0.05 (6)	0.95 ± 0.05 (9)
W California	0.48	0.93 ± 0.08 (10)	0.95 ± 0.07 (11)	0.94 ± 0.08 (21)
C California	0.50	0.97 ± 0.02 (6)	0.90 ± 0.09 (6)	0.94 ± 0.07 (12)
Mean (and total)	0.39	0.95 ± 0.06 (23)	0.90 ± 0.11 (36)	0.92 ± 0.10 (59)

$$+\frac{f}{S^2}(UUg + VVg) \qquad \text{(pressure)}$$

$$-f \qquad \text{(Coriolis)} \qquad (17)$$

(for the full derivation see Appendix D). Inspection of (17) suggests that the frictional term can be of the same order of magnitude as the other terms. Of course, a frictional parameterization which assumes a linear stress profile would neglect this contribution.

In order to assess the effect of a more accurate frictional force on hodograph shape, the following set of equations was solved:

$$\frac{\partial u}{\partial t} - fv = K\frac{\partial^2 u}{\partial z^2} - F_1(t), \qquad (18)$$

$$\frac{\partial v}{\partial t} + fu = K\frac{\partial^2 v}{\partial z^2} - F_2(t), \qquad (19)$$

where

$$\left.\begin{aligned} F_1(t) &= A\sin(\omega t - \alpha) \\ F_2(t) &= B\sin(\omega t - \beta) \end{aligned}\right\}, \qquad (20)$$

K is the eddy viscosity which is assumed constant, and α and β are phase shifts. The following initial and boundary conditions were assumed:

$$\left.\begin{aligned} &u(z, 0) = v(z, 0) = 0, \quad \text{at time } t = 0 \\ &u(0, t) = v(0, t) = 0 \\ &u(h, t) = v(h, t) = 0 \end{aligned}\right\}, \qquad (21)$$

where h is the height of the PBL.

The full derivation of the solution was achieved through Laplace transforms and is beyond the scope of this paper. The final results in complex notation may be written as

$$V(z, t) \equiv u(z, t) + iv(z, t)$$
$$= \frac{2}{\pi}\sum_{n=1}^{\infty}\frac{1}{2n-1}(E_{1n}e^{i\omega t} + E_{2n}e^{-i\omega t} - E_{3n}e^{-(C_n^2+if)t})\sin\frac{(2n-1)\pi}{h}, \qquad (22)$$

where

$$\left.\begin{aligned} C_n &= \sqrt{f}\frac{(2n-1)\pi}{h/D} \\ D &= \frac{K}{f}, \quad \text{frictional height} \\ E_{1n} &= \frac{iAe^{-i\alpha} - Be^{-i\beta}}{Cn^2 + i(f+\omega)} \\ E_{2n} &= \frac{-iAe^{i\alpha} + Be^{-i\beta}}{C_n^2 + i(f-\omega)} \\ E_{3n} &= E_{1n} + E_{2n} \end{aligned}\right\}. \qquad (23)$$

Figure 9 presents six hodographs that were calculated from (22). Their respective altitudes are 50, 100, 200, 300, 400 and 500 m, and we have assumed that the PBL height is 1000 m, $K = 1\ \text{m}^2\ \text{s}^{-1}$, $A = B = 4.8 \times 10^{-4}\ \text{m s}^{-2}$, $\alpha = 0°$, $\beta = 60°$, and latitude $\phi = 60°\text{N}$. The results are presented for 24 hours starting at $t = 500$ hours for which transient features completely disappear. The hodographs become quite stable after about two to three diurnal cycles. As illustrated in Fig. 9, ACR is reached at the lower levels of the PBL below ~300 m. Above this level the hodographs change to clockwise rotation. Similar behavior was also found in the numerical simulation (see Part I, Fig. 5, where the partly ACR surface hodograph in the lee of the mountain changes at ~200 m to a clearly CR hodograph). This example illustrates that, as with the Rayleigh friction, a relatively large phase shift ($\beta - \alpha = 60°$ in Fig. 9) between the horizontal thermal forces favors ACR. Also, it is interesting to note that the tilt angle is not much different than that predicted by the Rayleigh friction theory, i.e., $\alpha \approx 45 - \phi$, giving $-15°$ in this case). The eccentricity of the 50 m hodograph may be compared to that predicted by the Rayleigh friction theory for $k/\omega = 1$ or 2 (Figs. 2b or c, for $\theta = 60°$). It seems more appropriate to compare the lower eccentricity value for the second case ($k/\omega = 2$), $e \approx 0.9$, with the result presented by the K-theory hodograph ($K = 1\ \text{m}^2\ \text{s}^{-1}$).

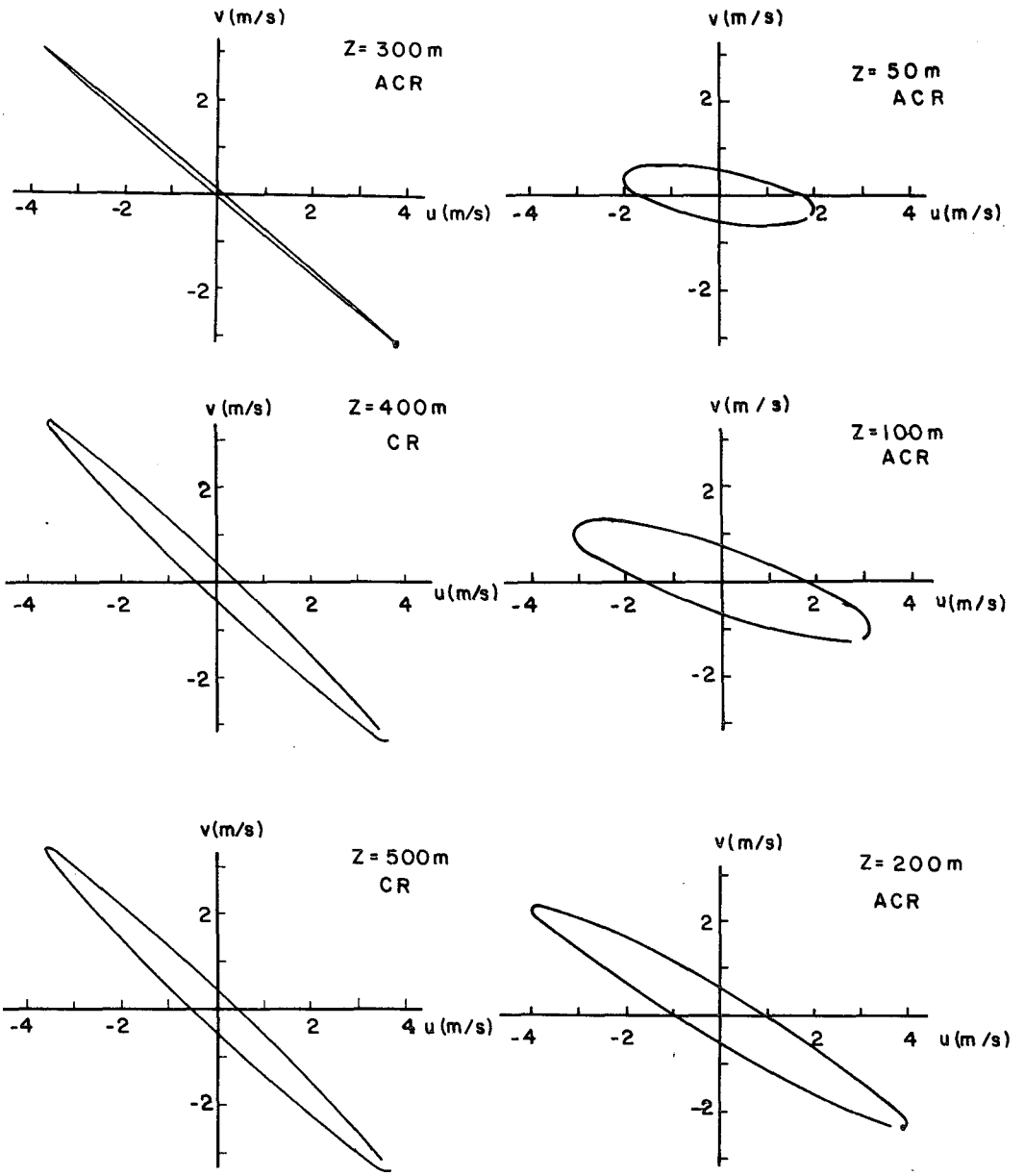

FIG. 9. Predicted hodographs at altitudes of 50, 100, 200, 300, 400 and 500 m with h = 1 km, K = 1 m^2 s^{-1}, $A = B = 4.8 \times 10^{-4}$ m s^{-2}, $\alpha = 0$, $\beta = 60°$ and $\phi = 60°$. Starting time is 500 h and ending time is 524 h.

A detailed study of eccentricity, tilt angle and sense of rotation for hodographs using the K-theory, and differences of these from Rayleigh friction theory on the one hand, and with a larger data base of observed hodographs on the other, is now being undertaken.

6. Discussion and conclusions

Zambakas (1973), in a study of 50 cases of diurnal sea breezes at Athens, concluded that the sea-breeze wind "backs (rotates in the ACR sense) in disagreement with the theory." In his discussion he suggested that the ACR was due to thermal forcing which arrived later in the day from the open sea (not from the nearest gulf) and was responsible for the ACR of the wind at Athens. The ACR rotation due to thermal forcing was included in the present theory (Part I of this study) and resulted in various ACR hodographs. The indented coastline was responsible for the ACR at Athens and probably also at Wick, northeast Scotland (Gill, 1968). These are only two additional examples of many observations that show ACR. In this work we concentrated on analyses of 47 stations in Washington and California plus an additional 12 stations in central California for which the sense of

rotation, eccentricity and tilt angle of the major axis were calculated and compared to the results predicted by the theory. The important results were as follows:

1) In the Northern Hemisphere, the frequency of ACR occurrences does not necessarily decrease northward. On the contrary, the linear theory suggests that there is some latitude, depending upon friction, at which a minimum ACR exists. As friction increases, this latitude moves northward. (It is thus true that for medium to high values of friction the frequency of ACR decreases northward.) The predicted curves for ACR frequency as a function of latitude were constructed, and most of the analyzed data seemed to be in agreement with them. Analyses of additional data for higher as well as lower latitudes are necessary in order to assess more accurately the applicability of these curves in the study of ACR frequency at different latitudes.

2) In linear theory the latitude ϕ has a major influence on the tilt angle α of the hodograph ellipse. In fact, the theory predicts a very simple relation at low and middle latitudes when assuming equal thermal forces in both horizontal directions. It was shown that in this case $\alpha \approx 45° - \phi$; this relation was found to be in accordance with the observed tilt angles in Washington and California. This result contrasts with the relation $\alpha \approx -\phi$ which was shown to hold in the case of one horizontal force ($B = 0$) at lower latitudes. The latter case corresponds to the Haurwitz (1947) theory. Recently we plotted α values of 68 analysed hodographs as a function of ϕ and tried to fit these with the line of least squares in order to assess the linear relationship between α and ϕ. Unfortunately the hodographs were restricted to latitudes between 36 and 51°N and no significant linear correlation could be shown with this data base. As pointed out by D. O. Staley (personal communication, 1983), the most striking variations of tilt angle and eccentricity with latitude should, if the theory could be validated, be found at low latitudes, or by comparison of low with high latitudes. However, only a few hodographs were available at high latitudes and nearly none for low latitudes. Of course, we should be aware of the highly simplified nature of the theory and the severe limitations imposed by it. Besides the simplified friction, the omission of linear advection due to the large-scale pressure gradient is apparently an important source of error in the calculation of the tilt angle of the hodograph. This angle might be considerably influenced by the different and nonzero average large-scale pressure gradient at each location.

3) In general, high values of eccentricity were predicted by the theory and the observed hodographs supported these results. Although the slight observed northward decrease in average eccentricity fits the theory, further data analyses are necessary before we can reach a more confident conclusion with regard to latitudinal behavior.

4) Nearly circular hodographs found in regions of expected high friction were shown by the present theory to result from a rotating thermal force. It was shown that low eccentricities are possible with realistic values of friction if a relatively large phase shift (between the horizontal thermal forces) exists. When a phase shift of $\theta = 90°$ was reached, circular hodographs were predicted no matter how large the friction became in the case of equal horizontal thermal forces (see Figs. 2b and c).

5) Highly elongated hodographs could be explained by the present theory even with relatively low friction depending strongly upon the phase shift θ. This might explain some of the very high eccentricities of observed hodographs at coastal stations which do not seem to be influenced by strong friction. See, for example, the July hodograph at Athens of Zambakas (1973), or the high eccentricity (1.0) at the Farallon Islands near the California coast (at the extreme bottom left of Fig. 5).

6) It was illustrated that the phase shift between the horizontal thermal forces plays a very important role in determining the sense of rotation (Fig. 4c).

7) The explicit contribution of the frictional force to the rate of wind rotation for a nonlinear stress profile was presented (following Wyngaard). A simple expression was given for the baroclinic convective PBL.

8) The momentum equations were solved with the height-dependent K-theory parameterization. It was shown that ACR surface hodographs resulted, with relatively high phase shifts between the thermal forces. The eccentricity of the ACR hodograph increased with height to the point where the hodograph changed its sense of rotation to become clockwise. With some typical parameters the conversion height was found to be ~300 m.

In summary, we would like to clarify the goal of our work. It is to better understand hodograph shapes and the physical reasons for them. We believe that the average wind hodograph can indicate the local thermal forcings which play a significant role in determining hodograph shape. The most important task, but also the most difficult to perform, is to develop a method which will enable us to get an idea about local thermal forcings based upon the hodograph, along with additional data (like pressure and temperature) that might be available. The main advantage of the wind hodograph is that it represents point data that are relatively easy to calculate but at the same time reflect, often quite clearly, the local thermal forcings. Such a method, if available, would be extremely useful for realistic initializations and parameterizations of numerical mesoscale models of the PBL.

Finally, it should be mentioned that this study was restricted to the Northern Hemisphere, especially with regard to hodograph tilt angles and eccentricities,

since appropriate Southern Hemisphere data were not available.

Acknowledgments. This research was partially supported by the National Science Foundation under Grant ATM 78-23330. P.A. conducted part of this work at the Cooperative Institute for Mesoscale Meteorological Studies, Oklahoma University. M.K. wishes to thank the government of Japan for supporting his stay at Harvard University as a visiting scholar.

We wish to express our gratitude to Professor Lindzen for supporting our research at the Center for Earth and Planetary Physics, Harvard University, and to Professors J. Neumann, M. Uryu and B. Gelchinsky for their interest and helpful remarks.

$$\tilde{u} = \frac{A}{2}\frac{(f^2-\omega^2-k^2)\omega\sin\omega t-(f^2+\omega^2+k^2)k\cos\omega t}{(f^2-\omega^2-k^2)^2+4k^2f^2} - \frac{B}{2}\frac{2kf\omega\sin(\omega t-\theta)+(f^2-\omega^2+k^2)f\cos(\omega t-\theta)}{(f^2-\omega^2-k^2)^2+4k^2f^2}$$

$$\tilde{v} = \frac{A}{2}\frac{2kf\omega\sin\omega t+(f^2-\omega^2+k^2)f\cos\omega t}{(f^2-\omega^2-k^2)^2+4k^2f^2} + \frac{B}{2}\frac{(f^2-\omega^2-k^2)\omega\sin(\omega t-\theta)-(f^2+\omega^2+k^2)k\cos(\omega t-\theta)}{(f^2-\omega^2-k^2)^2+4k^2f^2}$$

By some algebra, these expressions could be rewritten as

$$\left.\begin{aligned}\tilde{u} &= u_0\sin(\omega t+\lambda_u)\\ \tilde{v} &= v_0\sin(\omega t+\lambda_v)\end{aligned}\right\},$$

where

$$\left.\begin{aligned}u_0 &= (u_1^2+u_2^2)^{1/2},\quad \tan\lambda_u = u_2/u_1\\ u_1 &= AC_1 - BC_3\cos\theta - BC_4\sin\theta\\ u_2 &= AC_2 + BC_3\sin\theta - BC_4\cos\theta\\ C_1 &= (\omega/2D)(f^2-\omega^2-k^2)\\ C_2 &= (k/2D)(f^2+\omega^2+k^2)\\ C_3 &= 2fk\omega/2D\\ C_4 &= (f/2D)(f^2-\omega^2+k^2)^{-1}\\ D &= (f^2-\omega^2-k^2)^2+4f^2k^2\end{aligned}\right\}.$$

Similar expressions may be derived for v_0 and λ_v.

APPENDIX B

Derivation of a Criterion for Defining the Tilt Angle

Let α_1 be the angle of anticlockwise rotation of the coordinate system which will put the ellipse into a canonical form, i.e., major *or* minor axes coincide with the $\tilde{u}$ axis. There are only two possibilities if we require that $0 < \alpha_1 < 90°$: 1) The major axis coincides with $\tilde{u}$, so $\alpha = \alpha_1$. 2) The minor axis coincides with $\tilde{u}$; here, we should define $\alpha = \alpha_1 - 90°$ since it is the minor axis which makes an angle α_1 with the positive direction of the $\tilde{u}$ axis.

APPENDIX A

Derivation of Relations for $\tilde{u}$ and $\tilde{v}$

Kusuda and Alpert (1983) show that

In order to determine which case applies, let us turn to the equations (omitting the tildes)

$$\left.\begin{aligned}u &= u_0\sin(\omega t+\lambda_u)\\ v &= v_0\sin(\omega t+\lambda_v)\end{aligned}\right\}$$

which define the ellipse

$$v_0^2u^2 + u_0^2v^2 - 2u_0v_0\cos(\lambda_u-\lambda_v)uv - u_0^2v_0^2\sin^2(\lambda_u-\lambda_v) = 0.$$

When transforming this ellipse to a canonical form it may be shown that there are three cases:

$$\left.\begin{aligned}&1)\quad \alpha = \alpha_1 \Leftrightarrow \cos(\lambda_u-\lambda_v) > 0\\ &2)\quad \alpha = \alpha_1 - 90° \Leftrightarrow \cos(\lambda_u-\lambda_v) < 0\\ &3)\quad \alpha = 0 \Leftrightarrow \cos(\lambda_u-\lambda_v) = 0\end{aligned}\right\}.$$

On substituting λ_u and λ_v as derived in Appendix A, it is shown that

$$\cos(\lambda_u-\lambda_v) = \{-(A^2-B^2)fk + AB(-f^2+\omega^2+k^2)\cos\theta\}/(4Du_0v_0).$$

For the special case $B = 0$, equivalent to the Haurwitz (1947) theory, we find

$$\text{sign}\{\cos(\lambda_u-\lambda_v)\} = \text{sign}(-A^2fk) < 0$$

for northern latitudes. However, when $A = B \neq 0$ we get

$$\text{sign}\{\cos(\lambda_u-\lambda_v)\} = \text{sign}\{(k^2+\omega^2-f^2)\cos\theta\},$$

which for $k = \omega$ and $90° > \theta > -90°$ leads further to

$$\operatorname{sgn}\{\cos(\lambda_u - \lambda_v)\} = \operatorname{sgn}(2\omega^2 - f^2) = \begin{cases} + \text{ for } |\phi| < 45° \\ - \text{ for } |\phi| > 45°. \end{cases}$$

This means that α changes sign at $\pm 45°$ (where $f^2 = 2\omega^2$) as illustrated by Fig. 2b.

APPENDIX C

Derivation of Expressions for e and α

Following the definition of u and v (omitting the tildes) as

$$\left.\begin{aligned} u &= u_0 \sin(\omega t + \lambda_u) \\ v &= v_0 \sin(\omega t + \lambda_v) \end{aligned}\right\},$$

the tilt of the ellipse axis is given by

$$\tan 2\alpha = 2u_0 v_0 [\cos(\lambda_u - \lambda_v)]/(u_0^2 - v_0^2)$$

and

$$e = \sqrt{r}/a,$$

where

$$\left.\begin{aligned} r &= |u_0^2 - v_0^2|(1 + \tan^2 2\alpha)^{1/2} \\ a &= \{\sqrt{2} u_0 v_0 |\sin(\lambda_u - \lambda_v)|\}/(u_0^2 + v_0^2 - r)^{1/2} \end{aligned}\right\}.$$

Further substitutions for λ_u, λ_v, u_0 and v_0 (see Appendix A) lead to the final expressions (8) and (9).

APPENDIX D

The Contribution of Frictional Force to Wind Rotation

The following derivation is due to J. C. Wyngaard (personal communication, 1984). The equation for evolution of the surface wind angle α, when advection and terrain-slope effects can be neglected, is

$$\begin{aligned} \frac{d\alpha}{dt} &= \frac{1}{S^2}\left(U\frac{dV}{dt} - V\frac{dU}{dt}\right) \\ &= \frac{1}{S^2}\left(V\frac{\partial}{\partial z}\overline{uw} - U\frac{\partial}{\partial z}\overline{vw}\right) \quad \text{(friction)} \\ &\quad + \frac{f}{S^2}(UU_g + VV_g) \quad \text{(pressure)} \\ &\quad - f \quad \text{(Coriolis).} \end{aligned} \tag{D1}$$

The corresponding equations of motion are

$$\frac{\partial U}{\partial t} + \frac{\partial}{\partial z}\overline{uw} = f(V - V_g), \tag{D2}$$

$$\frac{\partial V}{\partial t} + \frac{\partial}{\partial z}\overline{vw} = f(U_g - U). \tag{D3}$$

Now we average (D2) and (D3) over the PBL, between a "surface-wind" height and the PBL top, where stress vanishes. We denote the PBL depth by h, averaged quantities by angular brackets, and surface quantities by subscript s. In quasi-steady conditions this gives

$$-\frac{\overline{uw}_s}{h} = f(\langle V\rangle - \langle V_g\rangle), \tag{D4}$$

$$-\frac{\overline{vw}_s}{h} = f(\langle U_g\rangle - \langle U\rangle). \tag{D5}$$

We decompose each variable into its layer mean plus a deviation, e.g.,

$$\frac{\partial}{\partial z}\overline{uw} = -\frac{\overline{uw}_s}{h} + \delta F_x, \tag{D6}$$

$$\mathbf{V} - \mathbf{V}_g = \langle \mathbf{V}\rangle - \langle \mathbf{V}_g\rangle + \delta \mathbf{V}_a. \tag{D7}$$

Using (D4)–(D7) in (D2) and (D3) then gives expressions for the stress divergence:

$$\frac{\partial}{\partial z}\overline{uw} = -\frac{\overline{uw}_s}{h} + f\delta V_a, \tag{D8}$$

$$\frac{\partial}{\partial z}\overline{vw} = -\frac{\overline{vw}_s}{h} - f\delta U_a. \tag{D9}$$

Thus the stress divergence is a constant plus a z-dependent deviation. If we parameterize the constant term through the surface wind, i.e.,

$$-\frac{\overline{uw}_s}{h} = \frac{C_D S_s U_s}{h}, \tag{D10}$$

$$-\frac{\overline{vw}_s}{h} = \frac{C_D S_s V_s}{h}, \tag{D11}$$

then we see by substitution into (D1) that the constant term does not contribute to the turning of the surface wind angle.

The height-dependent part of the stress divergence, (D8) and (D9), does give a frictional contribution to (D1):

$$\text{friction} = \frac{f}{S^2}(V\delta V_a + U\delta U_a). \tag{D12}$$

In general, we can rotate axes such that one of these terms, but not both, is zero.

It is thus suspected that the frictional term in (D1) vanishes if and only if the stress profile is linear; that is, if and only if the second terms on the right of (D8) and (D9) vanish. Thus friction should vanish in the barotropic convective PBL, but not in the neutral PBL, the stable PBL, or the baroclinic, convective PBL.

Consider the baroclinic, convective PBL. Assume that the wind profile remains flat in the presence of baroclinicity; thus the stress curvature balances the (constant) vertical shear in the pressure gradient:

$$\frac{\partial^2}{\partial z^2}\overline{uw} = -f\frac{\partial V_g}{\partial z}, \tag{D13}$$

$$\frac{\partial^2}{\partial z^2}\overline{vw} = f\frac{\partial U_g}{\partial z}. \tag{D14}$$

Integrating these and using the boundary conditions gives near the surface

$$\frac{\partial}{\partial z}\overline{uw} = -\frac{\overline{uw}_s}{h} + f\frac{\partial V_g}{\partial z}\frac{h}{2}, \quad \text{(D15)}$$

$$\frac{\partial}{\partial z}\overline{vw} = -\frac{\overline{vw}_s}{h} - f\frac{\partial U_g}{\partial z}\frac{h}{2}. \quad \text{(D16)}$$

Equation (1) then becomes

$$\frac{d\alpha}{dt} = \frac{fh}{2S^2}\left(V\frac{\partial V_g}{\partial z} + U\frac{\partial U_g}{\partial z}\right) \quad \text{(friction)}$$

$$+ \frac{f}{S^2}(UU_g + VV_g) \quad \text{(pressure)}$$

$$- f \quad \text{(Coriolis).} \quad \text{(D17)}$$

Inspection of (D17) shows that all three terms can be of the same order of magnitude. In fact, it can be written

$$\frac{d\alpha}{dt} = \frac{f}{S^2}(U\langle U_g\rangle + V\langle V_g\rangle) \quad \text{(pressure plus friction)}$$

$$- f \quad \text{(Coriolis),} \quad \text{(D18)}$$

which means that the friction term acts to make the layer behave as if it were barotropic, i.e., it senses the layer-averaged geostrophic wind.

REFERENCES

Barbato, J. P., 1978: Areal parameters of the sea breeze and its vertical structure in the Boston basin. *Bull. Amer. Meteor. Soc.*, **59**, 1420–1431.

Clarke, R. H., 1970: Observational studies in the atmospheric boundary layer. *Quart. J. Roy. Meteor. Soc.*, **96**, 91–114.

Fosberg, M. A., and M. J. Schroeder, 1966: Marine air penetration in central California. *J. Appl. Meteor.*, **5**, 573–589.

Frenzel, C. W., 1962: Diurnal wind variations in central California. *J. Appl. Meteor.*, **1**, 405–412.

Frizzola, J. A., and E. L. Fisher, 1963: A series of sea-breeze observations in the New York City area. *J. Appl. Meteor.*, **2**, 722–739.

Gill, D. S., 1968: The diurnal variation of the sea-breeze at three stations in north–east Scotland. *Meteor. Mag.*, **97**, 19–24.

Haurwitz, B., 1947: Comments on the sea-breeze circulation. *J. Meteor.*, **4**, 1–8.

Kusuda, M., and P. Alpert, 1983: Anti-clockwise rotation of the wind hodograph. Part I: Theoretical study. *J. Atmos. Sci.*, **40**, 487–499.

Mori, Y., 1982: On climatological aspects of daily variation of surface wind in Japan. Tenki, **29**, 223–230 (in Japanese).

Staley, D. O., 1957: The low-level sea-breeze of northwest Washington. *J. Meteor.*, **14**, 458–470.

——, 1959: Some observations of surface-wind oscillations in a heated basin. *J. Meteor.*, **16**, 364–370.

Thorpe, A. J., and T. H. Guymer, 1977: The nocturnal jet. *Quart. J. Roy. Meteor. Soc.*, **103**, 633–653.

Weber, M. R., 1978: Average diurnal wind variation in southwest lower Michigan. *J. Appl. Meteor.*, **17**, 1182–1189.

Wexler, R., 1946: Theory and observations of land and sea breezes. *Bull. Amer. Meteor. Soc.*, **27**, 272–287.

Zambakas, J. D., 1973: The diurnal variation and duration of the sea breeze at the national observatory of Athens, Greece. *Meteor. Mag.*, **102**, 224–228.